



## CHAOS AND PHASE SYNCHRONIZATION IN ECOLOGICAL SYSTEMS

BERND BLASIUS\* and LEWI STONE†

*The Porter Super-Center for Ecological and Environmental Studies,  
Tel Aviv University, Ramat Aviv, Tel Aviv 69978, Israel*

Received August 9, 1999; Revised October 27, 1999

An ecological population model is presented for the purposes of exploring complex synchronization phenomena in biological systems. The model describes a three level predator–prey–resource system which oscillates with Uniform Phase evolution, yet has Chaotic Abundance levels or Amplitudes (UPCA). We investigate the phase synchronization of two nonidentical diffusively coupled phase coherent models (i.e. with UPCA dynamics) and extend the analysis to study the models’ “funnel” regimes and response to noise forcing. Similar synchronization effects are reported for a two-dimensional lattice of chaotic population models coupled via nearest neighbors. With weak coupling, a collective phase synchronization emerges yet the peak population abundance levels are chaotic and largely uncorrelated. The synchronization patterns and traveling wave structures found in the spatial model correspond to those observed in natural systems — in particular, Ecology’s well-known Canadian hare–lynx cycle. We show that phase synchronization has important applications in the study of ecological communities where the spatial coupling of populations can lead to large scale complex synchronization effects.

### 1. Introduction

Synchronization is a fundamental phenomenon arising in many biological and physical contexts for which there are two or more coupled oscillating systems. In the classical sense, and dating back at least to Huygens in the 17th century [Huygens, 1673], synchronization has been understood as the mutual adjustment of periodic oscillators and the frequency locking that results because of their (often weakly) coupled interaction. Over the last decade, there has been considerable progress in generalizing this concept of synchronization to include the case of coupled chaotic oscillators. When the interaction of two nearly identical coupled chaotic systems is relatively strong, one observes “complete synchronization” i.e. the states of both systems become practically identical, while their dynamics in

time remains chaotic [Fujisaka & Yamada, 1983; Pikovsky, 1984; Pecora & Carroll, 1990]. This has been extended to the case of “generalized synchronization” where, although both states are quite different, there is nevertheless a direct functional relationship between them [Rulkov *et al.*, 1995].

An even more recent achievement has been the unveiling of the more subtle phenomenon of phase synchronization in nonidentical coupled chaotic systems [Rosenblum *et al.*, 1996; Pikovsky *et al.*, 1997]. Weak coupling causes the different chaotic systems to lock in phase to one another, while their amplitudes may remain chaotic and are, in general, uncorrelated. In some cases the phases of the signals are locked in a simple manner but often more complex relationships are to be expected and a statistical approach may be required for identification.

---

\*E-mail: bernd@lanina.tau.ac.il

†E-mail: lewi@lanina.tau.ac.il

Like many new notions, these more complex synchronization phenomena have been demonstrated mainly in idealized examples of simple model systems. Phase synchronization has been observed in mathematical models and laboratory studies of electronic circuits [Parlitz *et al.*, 1996] and there are indications that it occurs in ecological systems [Blasius *et al.*, 1999], climate systems [Palus, 1998] and in physiological data set, such as the human locomotory system and the human cardiorespiratory system [Schäfer *et al.*, 1998; Tass *et al.*, 1998].

In the present paper phase synchronization is investigated in the context of ecological and biological systems. We first formulate a simple foodweb model of a three species food-chain which generates phase coherent chaotic oscillations and is thus useful for exploring the synchronization of chaotic systems. Phase coherence guarantees that the populations oscillate at almost constant frequency which is characterized by a predominant peak in the power spectrum [Farmer *et al.*, 1980]. The model belongs to the class of phase coherent oscillators which have the property of Uniform Phase evolution, but nevertheless cycle with Chaotic Amplitudes (UPCA) (see Fig. 1). This type of oscillation is well known for a number of biological populations [Schaffer, 1984] which cycle with a seemingly constant frequency but have erratic peak population abundances [see e.g. Fig. 1(a)]. However, we know of no other biologically plausible model that is capable of producing the required UPCA oscillations.

Many examples of biological synchronization — some of them quite startling — have been documented in the literature, but currently theoretical understanding of the phenomena lags behind experimental and field-studies [Blasius & Stone, 2000]. Since weakly coupled chaotic systems with the property of UPCA are known to exhibit phase synchronization [Rosenblum *et al.*, 1996; Pikovsky *et al.*, 1997], the foodweb model provides the necessary framework for investigating the potential importance of this synchronization in biological systems. We proceed by coupling two foodweb models which might represent nearby patches or interacting communities. The coupled models show a whole range of synchronization transitions which match the dynamics reported in natural systems. In fact, the results of the model provides an intriguing interpretation of the unusual synchronization observed in Canada's hare-lynx cycle. This population

oscillation has been documented for over 100 years, with hare and lynx populations across Canada synchronizing in phase to a collective 10-year cycle that manifests over millions of square kilometers [see Sec. 6, Fig. 10(a)]. Similar spatially synchronized fluctuations have been observed across widely separated sites for many other ecological populations [Keith, 1963; Korpimäki & Krebs, 1996;

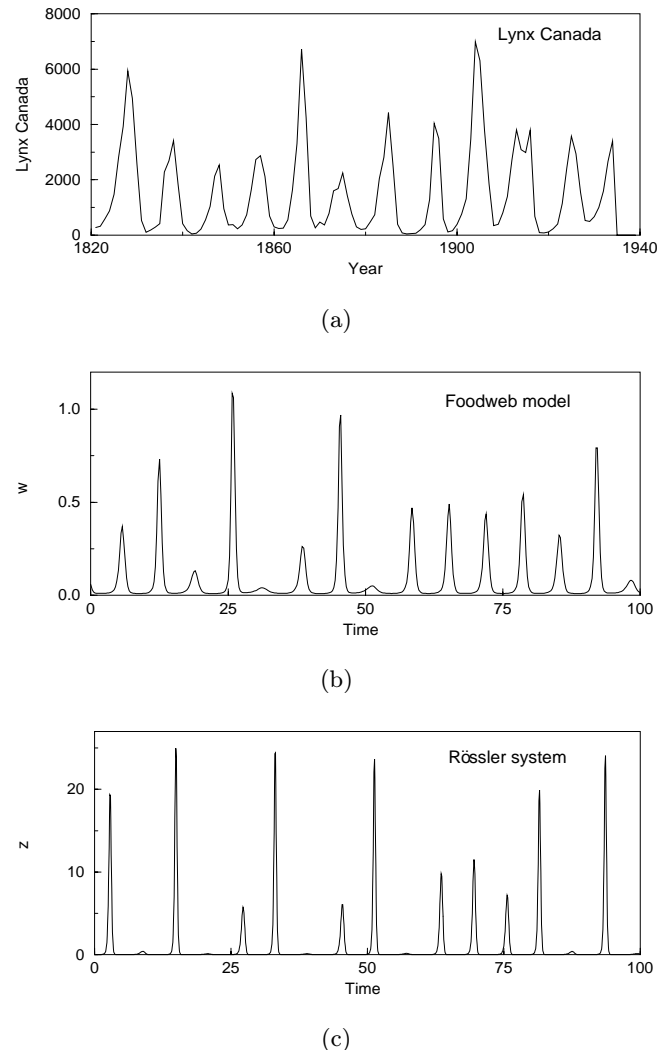


Fig. 1. (a) Ten-year cycle in the Canadian lynx in the Mackenzie river area (1821–1937) after [Elton & Nicholson, 1942]. (b) Chaotic time-series of top predator,  $w$ , in the foodweb model (1). For the simulations reported here, we used throughout the following parameters  $a = 1$ ,  $b = 1$ ,  $c = 10$ ,  $\alpha_1 = 0.2$ ,  $\alpha_2 = 1$ ,  $k_1 = 0.05$ ,  $k_2 = 0$ ,  $u^* = 0$ ,  $v^* = 0$ ,  $w^* = 0.006$ .  $f_1$  and  $f_2$  are taken as Holling type II and bilinear Lotka–Volterra interaction terms, respectively, although different combinations have been used successfully in other model variants [see e.g. Eq. (3)]. (c) Time-series of  $z$  in the Rössler system (2) for  $\gamma = 5.7$ . Initial transients in (b) and (c) have been removed.

Ranta *et al.*, 1997] and are also prominent in the dynamics of epidemic outbreaks as they spread between a network of neighboring cities [Levin *et al.*, 1997]. These examples motivate the extension of our analysis of the two-patch model to studying synchronization of an  $N \times N$  lattice system. We show that phase synchronization in spatial lattices can lead to unusual spatial chaotic wave structures that are found in natural systems.

The paper is organized as follows. In Sec. 2 we introduce and analyze the foodweb model, and compare it to other known UPCA systems such as the Rössler model. The phase evolution of these models and their respective funnel regimes are investigated in Sec. 3. In Sec. 4 a study is made of the synchronization transitions in two diffusively coupled UPCA models, and we focus on the occurrence and characterization of phase synchronization. Methods for detecting synchronization are also outlined. In Sec. 5 the influence of noise forcing on the foodweb model is investigated and we characterize noise-induced UPCA oscillations as well as the effects of noise on synchronization. In Sec. 6 we investigate how phase synchronization manifests in spatially extended systems. The results are discussed in Sec. 7.

## 2. An Ecological UPCA Model

Many ecological and biological populations that cycle in time have the unusual property that their period length remains remarkably constant while their abundance levels are highly erratic [Schaffer, 1984]. Figure 1(a) demonstrates these features for one of the most celebrated time-series in Ecology — the Canadian hare–lynx cycle. The behavior is reminiscent of the Rössler oscillator which has Uniform Phase evolution but Chaotic Amplitudes (UPCA) [Rössler, 1976; Farmer, 1981] — properties which have been the basis for a number of recent studies on phase synchronization [Rosenblum *et al.*, 1996, 1997; Osipov *et al.*, 1997].

However it is difficult to formulate or write down new equations, other than the (ecologically implausible) Rössler system, which exhibit UPCA, particularly if reasonable ecological or biological constraints are required. Our goal is to design and investigate a simple ecological foodweb model that exhibits UPCA. Consider the following equations

[Blasius *et al.*, 1999]

$$\begin{aligned}\dot{u} &= a(u - u^*) - \alpha_1 f_1(u, v) \\ \dot{v} &= -b(v - v^*) + \alpha_1 f_1(u, v) - \alpha_2 f_2(v, w) \\ \dot{w} &= -c(w - w^*) + \alpha_2 f_2(v, w).\end{aligned}\quad (1)$$

The model describes a standard three level “vertical” food chain, where the resource or vegetation  $u$  is consumed by herbivores  $v$ , which in turn are preyed on by top predators  $w$ . Note that  $u$ ,  $v$  and  $w$  might represent appropriately scaled population abundances or biomass levels. The coefficients  $a$ ,  $b$  and  $c$  represent the respective net growth rates of each individual species in the absence of interspecific interactions ( $\alpha_1 = \alpha_2 = 0$ ). The functions  $f_i(x, y)$  describe interactions between species with strengths  $\alpha_i$ . Predator–prey and consumer–resource interactions, are incorporated into the equations via the standard Lotka–Volterra term  $f_i(x, y) = xy$  or the Holling type II term  $f_i(x, y) = xy/(1 + k_i x)$ . We also assume the existence of a (stable or unstable) fixed point  $(u^*, v^*, w^*)$  in the absence of species interactions, and expand the system linearly around this steady state. The main difference between the present model and other standard Lotka–Volterra models [May, 1974; Hastings & Powell, 1991] is that here the steady state  $(u^*, v^*, w^*)$  is not necessarily set at the origin.

Despite its minimal structure, the equations capture complex dynamics including equilibrium and limit cycle behavior, as well as large parameter ranges for which there are well-defined chaotic oscillations. Figure 1(b) provides a time-series of a typical model run in the phase coherent chaotic regime. Observe that the top predator,  $w$ , oscillates at what appears to be a constant frequency although the maximum or peak amplitude of each cycle is highly unpredictable. These UPCA attributes of the model have much in common with the Canadian hare–lynx system as seen by comparing the real and simulated population trajectories in Figs. 1(a) and 1(b). The time-series of the foodweb model also resembles the UPCA found in the standard phase coherent Rössler system [Rössler, 1976] [see Fig. 1(c)]

$$\begin{aligned}\dot{x} &= -(y + z), \quad \dot{y} = x + 0.2y, \quad \dot{z} = 0.2 + z(x - \gamma).\end{aligned}\quad (2)$$

However the UPCA property alone is not sufficient to completely describe the dynamics of the observed data. Other factors that are of relevance include

the peak to peak variability and the changes in the peak to trough ratio of the cycle. For the hare-lynx system and other mammal populations in the boreal forests of North America, Korpimaki and Krebs [1996] suggested that the peak to trough ratio varies from 15–200  $\sim 1 : 13$ , a range that is very close to that found in the above foodweb model. In fact for the parameters given in Fig. 1(b), the ratio ranges between 4–120  $\sim 1 : 30$ . However the Rössler model with  $\gamma = 5.7$  has a peak to trough ratio that varies between 3.7–1770  $\sim 1 : 478$  i.e. one order of magnitude larger. In this respect the  $z$  variable of the Rössler system gives a rather poor description of the observed population cycles because its variability is much too high. Furthermore, there is no straightforward method to reduce the variability in the Rössler system without introducing other unrealistic features. For example, while a reduction in the bifurcation parameter  $\gamma$  reduces the peak to trough ratio, the peaks of the chaotic cycle become less uniformly distributed and instead, begin to resemble a periodic cycle. By lowering  $\gamma$  below  $\gamma = 5.7$ , the periodic regime of the Rössler systems is approached and the model cycles chaotically between a set of  $2^n$  small bands where the integer  $n$  decreases with  $\gamma$  [Farmer, 1981].

Figure 2(a) shows the phase coherent attractor of the foodweb model projected onto the  $(u, v)$ -plane. The attractor is very similar to that of

the Rössler equations ( $\gamma = 5.7$ ), and the regular cycling in the  $(u, v)$ -plane indicates strong phase coherency. As in the Rössler system, slight changes in parameter values can drive the foodweb model into a so-called “funnel regime” [Fig. 2(b)] [Farmer, 1980; Stone, 1992] which has a more complicated phase plane structure consisting of small and large loops, and weaker phase coherence.

The mechanism giving rise to UPCA dynamics is almost the same for both the Rössler and foodweb model as can be seen by comparing the two systems as follows. The simplest form of the foodweb model (1) that results in UPCA oscillations requires only Lotka–Volterra interactions, ( $k_i = 0$ ) (e.g. take  $a = 1, b = 1, c = 10, \alpha_1 = 0.1, \alpha_2 = 0.6, u^* = 1.5, v^* = 0, w^* = 0.01$ , see [Blasius & Stone, 1999]). Now rewrite Eqs. (1) and (2) in the following way

$$\begin{aligned} \dot{y} &= x + 0.2y & \dot{u} &= u(a - \alpha_1 v) - au^* \\ \dot{x} &= -y + z; & \dot{v} &= -v(b - \alpha_1 u + \alpha_2 w) \\ \dot{z} &= -z(5.7 - x) + 0.2 & \dot{w} &= -w(c - \alpha_2 v) + cw^*. \end{aligned} \tag{3}$$

The heart of the chaotic Rössler system is the neutrally stable harmonic cycle  $\dot{y} = x, \dot{x} = -y$  in the  $(x, y)$ -plane, which is made unstable by the linear negative damping term  $0.2y$ . The variables  $x$

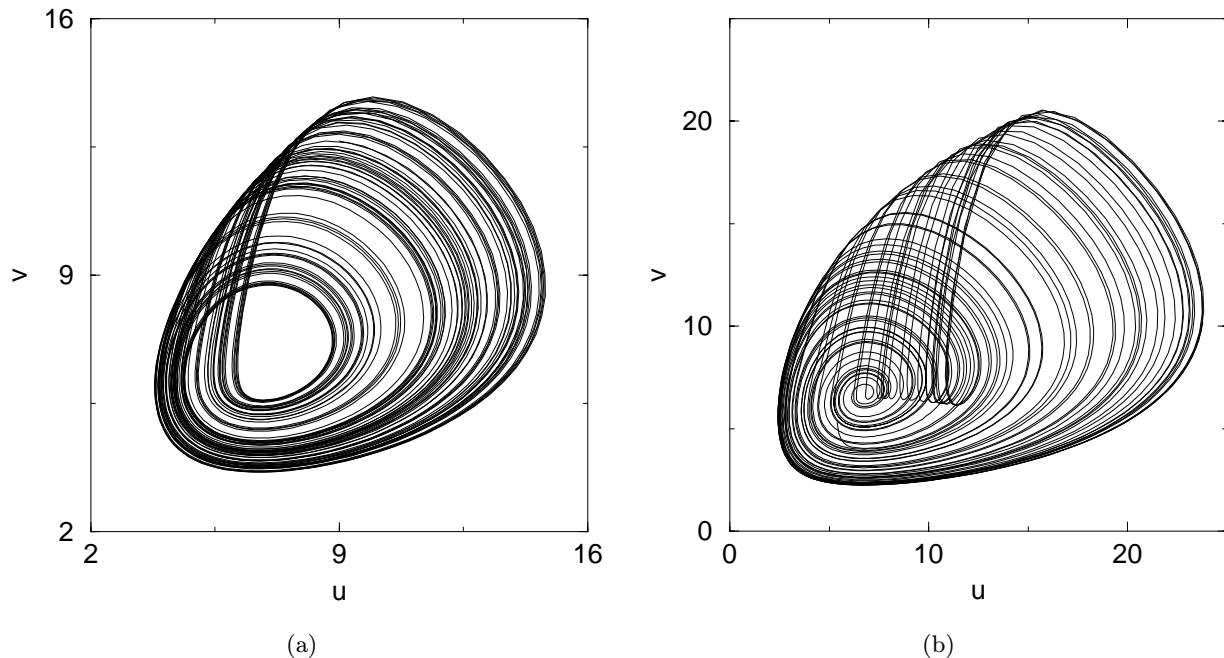


Fig. 2. Trajectories of the foodweb model (1) in the  $(u, v)$ -plane. (a) Phase coherent attractor for  $c = 10$ ; (b) “funnel” attractor for  $c = 12.3$ . Other parameters as in Fig. 1(b).

and  $y$  oscillate taking both positive and negative values, a feature that is unsuitable for a population model where variables should be strictly non-negative. Similarly, the basis of the chaotic foodweb model is the neutrally stable Lotka–Volterra cycle

$$\dot{u} = u(a - \alpha_1 v), \quad \dot{v} = -v(b - \alpha_1 u). \quad (4)$$

With positive initial conditions, the solution will always lie in the positive quadrant as required for a population model. In analogy to the Rössler system, instability (as may be evaluated through fixed point linearization) may be introduced into the Lotka–Volterra cycle. The two simplest methods we found required: (a) incorporating the

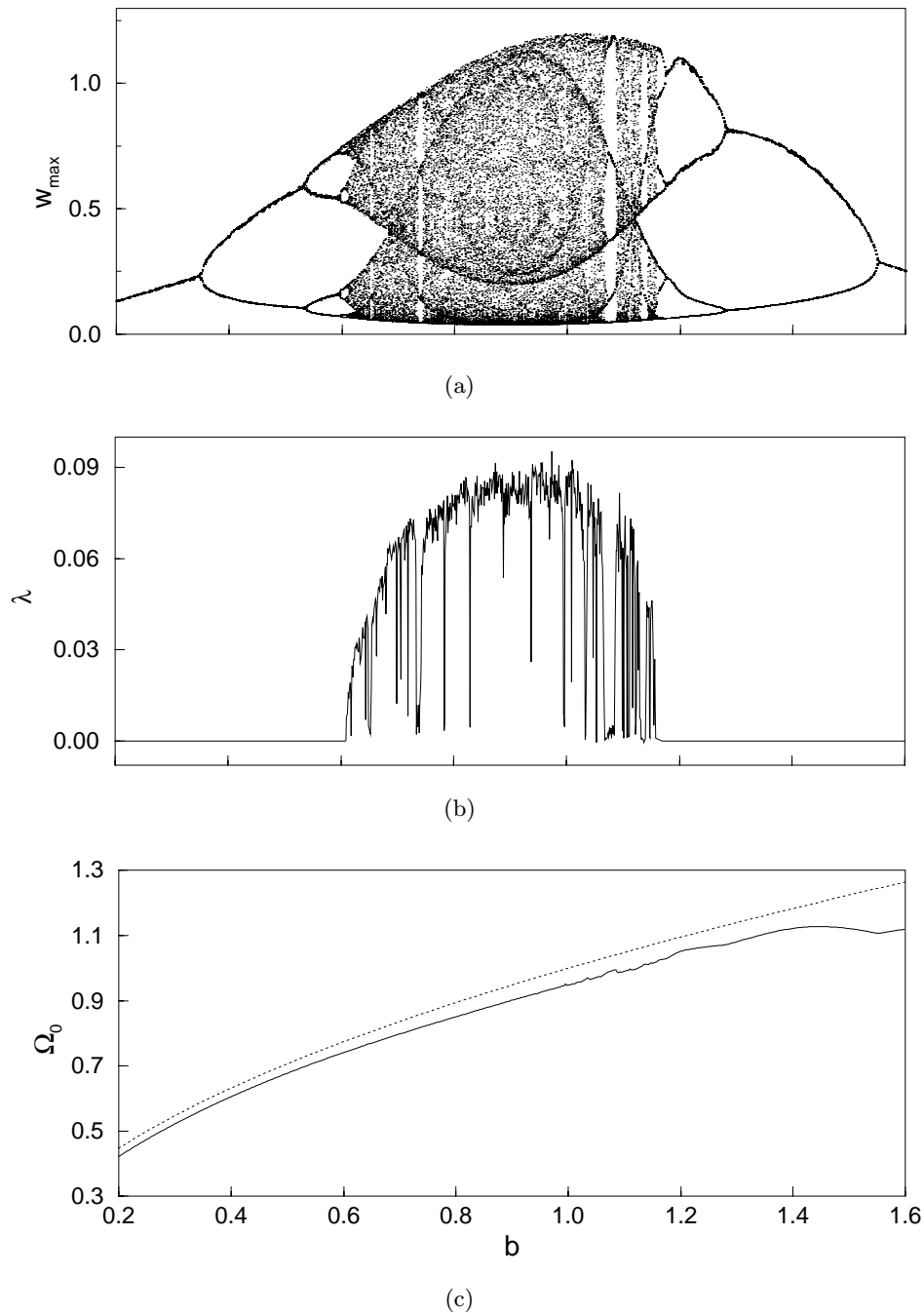


Fig. 3. Dynamics of the foodweb model (1) in the phase coherent regime ( $c = 10$ ) as a function of the control parameter  $b$ . (Other parameters as in Fig. 1(b).) (a) Bifurcation diagram; (b) largest Lyapunov exponent  $\lambda$ ; (c) numerically determined mean frequency  $\Omega_0$  (solid line). The approximation of the mean frequency  $\Omega_0(b) = \sqrt{b}$  (dotted line).

constant  $au^*$  in Eq. (3); or (b) incorporating a saturation in the consumption rate in the predator–herbivore  $(u, v)$  interaction, e.g. by replacing the simple Lotka–Volterra coupling with the more ecologically realistic Holling type II interaction [Blasius *et al.*, 1999].

The above discussion was concerned with only the first two equations of the Rössler and foodweb models. The third equation of the Rössler system, which describes the excursions of a (positive) spiky variable extending into the direction of a third ( $z$ ) axis, causes folding within the attractor — a prerequisite for chaotic dynamics. Upon examining Eqs. (3) one sees that the third equation of the Rössler system is in fact identical in structure to its counterpart in the foodweb model. The manner in which the third variable  $w$  feeds back into the  $(u, v)$ -plane of the foodweb model is again similar to the Rössler equations but modified to a Lotka–Volterra term,  $-a_2vw$ , typical for ecological predator–prey interactions.

In Fig. 3(a) we provide a bifurcation diagram of the foodweb model where the herbivore growth rate  $b$  is used as a control parameter. The diagram is constructed by plotting only the maxima of the predator variable,  $w$ , and makes clear a period-doubling route to chaos followed by a period-doubling reversal [Stone, 1993] as the control parameter  $b$  is increased. In Fig. 3(b) the largest Lyapunov exponent (LE) is plotted for the foodweb model, as a function of the control parameter  $b$ . The LE is positive and hence the dynamics chaotic, in exactly the same regions predicted by the bifurcation diagram. The frequency of the foodweb model’s cycle [as calculated below via Eq. (8)] is a monotonically increasing function for almost the entire range of the control parameter examined, as indicated in Fig. 3(c). In fact, the frequency of the foodweb model is largely determined by the underlying Lotka–Volterra cycle in the  $(u, v)$ -plane, given by Eq. (4), whose intrinsic frequency  $\Omega_0 = \sqrt{ab}$ . Figure 3(c) shows that this simple formula estimates well the mean frequency of the chaotic three variable system.

### 3. Phase Evolution of the Foodweb Model

In order to study the phase synchronization of complex systems, it is important to develop a means for decomposing a chaotic signal into its phase

and amplitude components. This is nontrivial for chaotic systems where often there is no unambiguous definition of phase. One general approach has been based on the analytical signal concept where the phase of a signal is obtained by the Hilbert transform [Gabor, 1946; Yalcinkaya & Lai, 1997; Rosenblum & Kurths, 1998].

For phase coherent models, the phase can be computed from geometric considerations using the formula  $\phi(t) = \arctan [(v(t) - \tilde{v}) / (u(t) - \tilde{u})]$ , where  $(\tilde{u}, \tilde{v})$  is a conveniently chosen point (e.g. unstable fixed point) interior to the coherent cycle in the  $(u, v)$ -plane. The shortcoming of this approach is that it is difficult to implement on measured scalar time-series of a single variable. In such applications attractor reconstruction techniques [Takens, 1981] are required to generate a second variable. Furthermore, if the data is spiky, as is the case of  $w$  in Eq. (1) (see Fig. 1), it becomes difficult to reconstruct (e.g. by time-delay coordinates or Hilbert transform) the smooth circular phase–plane structure required to define the phase by the above formula. Log-transforming the time-series may reduce this difficulty, but in practice this can lead to spurious results for “spiky” signals, especially if the data is chaotic.

We therefore make use of an alternative method that allows analysis and comparison of both model and observed data-sets even if the signal is “spiky”. In this scheme the instantaneous phase  $\phi(t)$  is defined from a knowledge of the time intervals between the spikes or maxima of, say, the top predator population  $w$ . Since we know the time  $t_n$  at which the top predator  $w$  reaches its  $n$ th maxima, and since the phase increases  $2\pi$  between successive maxima, linear interpolation can then be used to obtain the phase for intermediate times [Pikovsky *et al.*, 1997]. Thus

$$\phi(t) = 2\pi \frac{t - t_n}{t_{n+1} - t_n} + 2\pi n, \quad t_n < t \leq t_{n+1}. \quad (5)$$

Formula (5) gives a continuous piecewise-linear description of the phase. For purposes of studying long-term phase evolution and synchronization effects it is often sufficient to analyze the phase and amplitudes at discrete time intervals. In this case, it is useful to define the series of phases  $\phi_n = \phi(t_n) = 2\pi n$  so that the phase dynamics are obtained directly from times  $t_n$  of the maxima. The discrete amplitudes  $A_n$  are defined as the values of  $w$  at these maxima i.e.  $A_n = w(t_n)$ . The period

lengths between successive maxima are then given by  $T_n = t_{n+1} - t_n$  and instantaneous frequencies can be defined as  $\Omega_n = 2\pi/T_n$ .

In Fig. 5(a) we make use of Eq. (5) to evaluate the instantaneous phase of the foodweb model (1) and of the Lynx data (Fig. 1). In both cases we find an almost linear growth in the phase evolution. Nevertheless, small irregular fluctuations from the mean growth can be seen. Monitoring the phase evolution in this way is proving to be a very useful technique for analyzing biological time-series [Rosenblum & Kurths, 1998; Blasius *et al.*, 1999].

Our numerical simulations show that in terms of the discrete variables  $A_n$  and  $T_n$ , the dynamics of the foodweb model are well described by a two-dimensional discrete map [Farmer, 1981]

$$\begin{aligned} A_{n+1} &= F(A_n) \\ T_n &= G(A_n). \end{aligned} \quad (6)$$

Here  $F$  is the usual return map for the model's peak amplitudes  $A_n$ . The function  $G$  relates the peak amplitude to the period length  $T_n$  of the following cycle, thus providing some indication of how the amplitude dynamics of the chaotic model affects the phase dynamics. After numerically calculating  $A_n$  and  $T_n$  from time-series produced by the foodweb model, the functions  $F$  and  $G$ , were reconstructed, as shown in Fig. 4 for the model's phase coherent and funnel regimes. The functions  $F$  and  $G$  were also numerically derived for the phase coherent and funnel Rössler system and closely resembled the maps of the foodweb model. Note that  $F$  is a smooth single humped map and can be very well approximated with the well-known Ricker equation  $A_{n+1} = CA_n \exp(r(1 - A_n))$  [ $r = 6.2$ ,  $C = 0.04$  in Fig. 4(a)]. The close similarity between the peak to peak map of the foodweb model and the Ricker map is very interesting, since the Ricker map is a standard model used to describe chaotic population fluctuations. The tail like structure of the map at high amplitudes  $A_i$  leads to the period-doubling reversal seen in the bifurcation diagram [Fig. 3(a)] [Stone, 1993].

The discrete amplitude dynamics of the phase coherent and funnel regimes are very similar except that for the funnel, the tail of the map  $F$  (i.e. at large amplitudes) is characterized by a regime with a gently increasing slope. This is the signature of the distinctive small loops that appear in the funnel attractor [see Fig. 2(b)], which are triggered whenever the amplitude is larger than a certain threshold

level. These large amplitude levels do not arise in the phase coherent regime.

The most important difference between the phase coherent and the funnel regime is found in the phase dynamics. The function  $G$  associated with the funnel, is bimodal and characterized by two dominant period lengths that are to be associated with the large and small loops seen in the phase plane dynamics of Fig. 2(b). In the funnel regime  $G$  can be crudely approximated with a Heaviside step function [ $T_n = 7.1 - 4.1\mathcal{H}(A_n - 2.1)$  in Fig. 4(d)]. In the phase coherent regime  $G$  is a gradually decreasing function [Fig. 4(c)] that can be well approximated by a cubic function. If the oscillations were perfectly phase coherent,  $T_n$  would be a constant and  $G$  a horizontal straight line. The deviation of  $G$  from the horizontal is thus an indication of phase coherency and the strength of the interaction between amplitude and phase.

As seen from Fig. 4, the maxima  $A_i$  define in a unique way the period length of the following cycle  $T_n$  through the map  $G$ . This relationship can be used to calculate the period length of the preceding cycle  $T_{n-1} = G(F^{-1}(A_n))$ . However, the latter relationship is not well defined since here  $F$  is not an invertible function. It is thus impossible to directly predict the preceding period  $T_{n-1}$  from  $A_n$ , even if the maps  $F$  and  $G$  are known in advance.

In the case of the phase coherent foodweb model (1),  $G$  is an invertible function. This can be taken advantage of when deriving a return map for the periods  $T_n$

$$T_{n+1} = H(T_n) = GFG^{-1}(T_n). \quad (7)$$

Hence, in principle, it is possible to replace Eqs. (6) with two return maps  $A_{n+1} = F(A_n)$  and  $T_{n+1} = H(T_n)$  for the amplitudes and phases, and clearly demonstrates that the amplitude and phase dynamics can be decomposed in the foodweb model. Our numerical investigations of many different systems, including for example the Rössler system (2), have shown that, in general, the map  $G$  is not invertible and the dynamics cannot be decomposed in the same way. In these systems  $T_{n+1}$  cannot be calculated from  $T_n$  without additional knowledge of the amplitudes. Nevertheless, we cannot rule out the possibility that different decomposition schemes (e.g. via other Poincaré maps) might be more successful in these cases [Stone, 1992].

Given the sequence  $t_n$ , the times of peak amplitudes or maxima, the mean frequency  $\Omega_0$  can

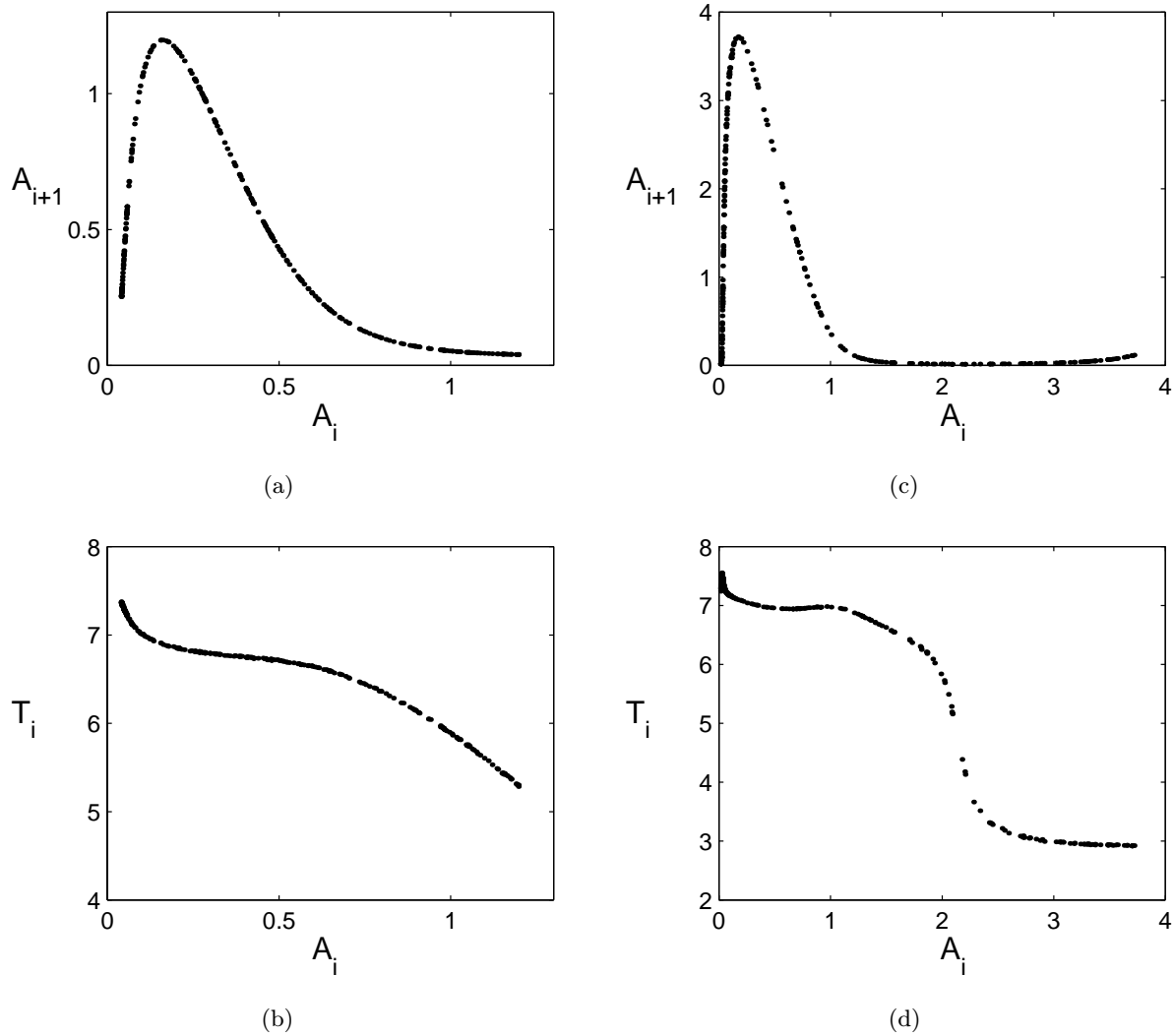


Fig. 4. Return map,  $A_{i+1} = F(A_i)$ , (top) and amplitude dependence of period length,  $T_i = G(A_i)$ , (bottom) of the foodweb model (1). Left column: phase coherent regime,  $c = 10$ ; right column: funnel regime,  $c = 12.3$ .

be simply defined as

$$\Omega_0 = \lim_{N \rightarrow \infty} 2\pi \frac{N - 1}{t_N - t_1} = \frac{2\pi}{\langle T_n \rangle}. \tag{8}$$

The formula is used to calculate the mean frequency of the foodweb model as a function of  $b$ , as plotted in Fig. 3(c). Note that  $\Omega_0$  also describes the mean phase growth of the foodweb model and corresponds to the slope of the phase evolution seen in Fig. 5(a). The small irregular deviations from the mean phase growth are also apparent and are a consequence of imperfect phase coherence. Equation (8) is also useful for analyzing measured data. For the Canadian Lynx cycle [Fig. 1(a)] we find a mean frequency of  $\Omega_0 = 0.66y^{-1}$ , which corresponds to a mean period of  $T_0 = 9.5$  years.

We turn now to examine ways of characterizing the degree of phase coherency in UPCA models. A

convenient measure is  $\sigma_T$ , the standard deviation of the time-intervals  $T_i$  as a percentage of the mean i.e.  $\sigma_T = 100 \cdot \sigma(T_i) / \langle T_i \rangle$ . For the parameterization used in Fig. 1 the series  $T_i$  has  $\sigma_T = 8.4\%$  for the foodweb model and  $\sigma_T = 7.99\%$  for the Rössler system. These large fluctuations of the period length with deviation of nearly 10% seemingly stand in contrast with our notion of uniform phase evolution. However, a calculation shows that the standard deviation,  $\sigma_\tau$ , of the two consecutive cycles  $\tau_i = T_{i+1} + T_i = t_{i+1} - t_{i-1}$  is much smaller than  $\sigma_T$ . Note that if  $T_i$  and  $T_{i+1}$  were independent random variables we would expect  $\sigma_\tau = \sqrt{2}\sigma_T$ . In fact we find  $\sigma_\tau = 3.99\%$  for the foodweb model and  $\sigma_\tau = 4.13\%$  in the Rössler system. This low variability is due to an unusual compensation effect that acts to maintain uniform phase evolution. As Fig. 4 reveals,



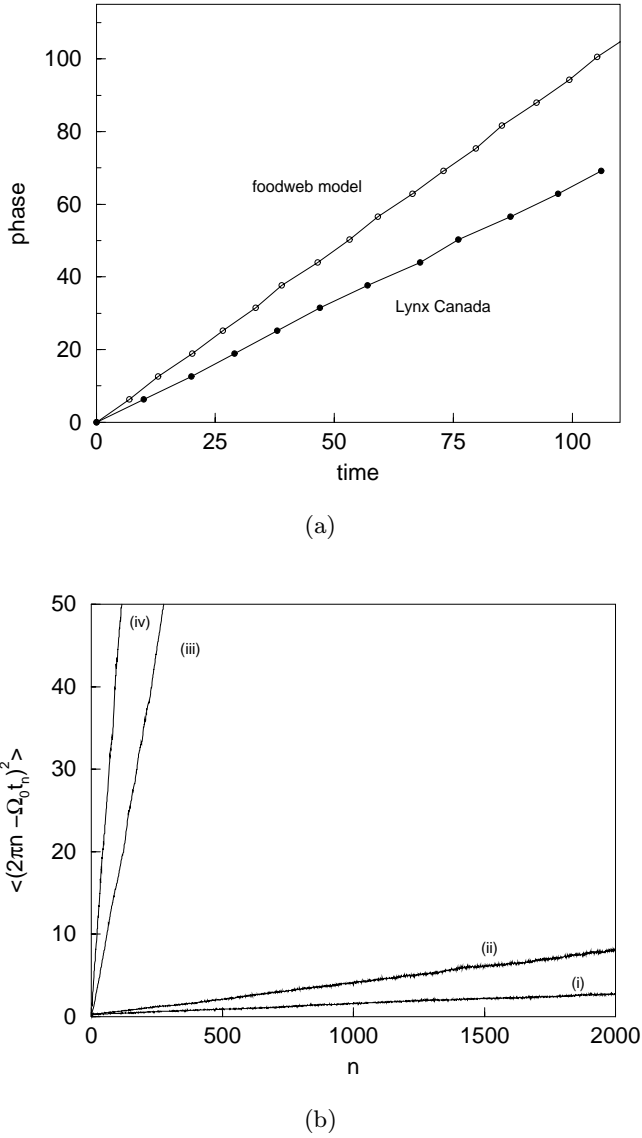


Fig. 5. (a) Phase evolution [determined by Eq. (5)] of the Canadian Lynx cycle (Fig. 1) (filled circles) and of the foodweb model (1) (open circles). The circles indicate the discrete phases  $\phi_n$  at times  $t_n$ . (b) Phase diffusion. Time evolution of the variance of  $\phi_n$ , Eq. (9), for (i) the Rössler system (2); (ii) the phase coherent foodweb model (1) with  $c = 10$ ; (iii) the noise forced foodweb model ( $D = 0.06$ ) parameterized on the limit cycle ( $b = 0.2, c = 10$ ); and (iv) the funnel regime of the strict deterministic foodweb model,  $c = 11.8$ .

a high amplitude  $A_i$  will always be accompanied by a short period  $T_i$  [see Fig. 4(a)] and yet, will also lead to a small peak  $A_{i+1}$  [Fig. 4(b)] with corresponding large period length  $T_{i+1}$ . Short periods are thus typically followed by long periods and vice versa which results in a more uniform phase evolution than the standard deviation of  $T_i$  suggests. The compensation is a result of the folding in the geometry of the Rössler-like attractor.

This motivates measuring the coherence of phase evolution by examining the variance of  $t_n = \sum_{k=1}^n T_k$  [Farmer, 1981], which is, up to a factor, directly related to the variance of  $\phi_n$ . As shown in [Farmer, 1981], the phase undergoes a random walk about the steady drift  $\Omega_0 t$  with a variance  $\langle (\phi - \langle \phi \rangle)^2 \rangle$  that increases linearly with  $t$ . The linear increase is measured by a diffusion constant  $D_\phi$ . In terms of the discrete phases

$$\langle (2\pi n - \Omega_0 t_n)^2 \rangle = 2\pi D_\phi t_n. \quad (9)$$

In Fig. 5(b) we compare the growth in the variance of the phase evolution for the phase coherent and “funnel” systems using the dimensionless scaled diffusion constant  $\tilde{D}_\phi = D_\phi/\Omega_0$ . Very small values of phase diffusion were found in both the phase coherent foodweb model ( $c = 10$ ) with  $\tilde{D}_\phi = 0.004$ , and Rössler system with  $\tilde{D}_\phi = 0.0012$ . In contrast, the funnel regime of the foodweb model had much larger phase diffusion with  $\tilde{D}_\phi = 2.55$  (not plotted) when  $c = 12.3$ , and  $\tilde{D}_\phi = 0.406$  for  $c = 11.8$  (plotted). Thus the “funnel” regime has a phase diffusion which is some three to four orders of magnitude larger than that of the phase coherent regime.

#### 4. Phase Synchronization in Two Coupled Systems

The foodweb model accounts for the UPCA dynamics of a single community. Our goal is to understand if and how two coupled oscillating foodweb models will synchronize. In this scenario, the two foodweb models might represent different patches or communities coupled together via diffusive migration. We suspect that the migration should act as a powerful synchronizing agent between populations which are spatially structured in patches or local assemblages. Previous modeling efforts have borne this out for simple systems with identical population dynamics. However, very little is known about the synchronization of chaotic and nonidentical population models. We first write down the equations for an arbitrary number of coupled patch models although in this section the analysis will be restricted to the case of two coupled systems. The coupled system (1) reads as follows:

$$\begin{aligned} \dot{u}_i &= a(u_i - u^*) - \alpha_1 f_1(u_i, v_i) \\ \dot{v}_i &= -b_i(v_i - v^*) + \alpha_1 f_1(u_i, v_i) \\ &\quad - \alpha_2 f_2(v_i, w_i) + \varepsilon \sum_j (v_j - v_i) \end{aligned} \quad (10)$$

$$\dot{w}_i = -c(w - w_i^*) + \alpha_2 f_2(v_i, w_i) + \varepsilon \sum_j (w_j - w_i)$$

where  $u_i$ ,  $v_i$  and  $w_i$  represent the vegetation, herbivore and predator populations in patch- $i$ , and  $\varepsilon$  sets the magnitude of diffusive migration summed over a predefined set of local nearest neighbors  $\{j\}$ . For biological reasons we allow migration for the mobile animal species only and consequently couple the  $v_i$  and  $w_i$  variables, although similar results are obtained if the  $u_i$  variables are also coupled. On the other hand if the top predators,  $w_i$  are coupled alone or with different coupling strength compared to the migration between the other species ( $u_i$  and  $v_i$ ), very complicated transitions to synchronization can arise [Blasius *et al.*, 1999]. The systems are assumed to be nonidentical and to cycle with different natural frequencies, which are determined by the coefficients  $b_i$ .

A simple but very useful index that helps in identifying synchronization in the coupled foodweb models is the relative frequency difference,  $\Delta\Omega$ . If the two foodwebs oscillate with frequencies  $\Omega_1$  and  $\Omega_2$  then  $\Delta\Omega = 2[(\Omega_2 - \Omega_1) / (\Omega_2 + \Omega_1)]$ , which is the frequency difference as a percentage of the average mean frequency. Naturally, if the two systems are frequency locked  $\Omega_1 = \Omega_2$  and  $\Delta\Omega = 0$ . Note that  $\Delta\Omega = \Delta\Omega(\varepsilon)$ , is a function of the coupling parameter  $\varepsilon$ . In practice,  $\Delta\Omega(\varepsilon)$  may be found numerically by first integrating out the patch models for a given coupling  $\varepsilon$ , using Eq. (8) to calculate the mean frequencies ( $\Omega_1, \Omega_2$ ), and this directly yields  $\Delta\Omega(\varepsilon)$ .

First we study the synchronization of two coupled patch systems in the phase coherent regime ( $c = 10$ ). Growth rates of consumers  $v_{1,2}$ , are given by  $b_{1,2} = b_0 \pm \Delta/2$ , where  $b_0 = 0.86$  and the models are deep in the chaotic regime when  $\Delta = 0$ , and reasonably far from the relatively large periodic windows of short or moderate periods [see Fig. 3(b)]. In the case of no coupling or migration the relative frequency difference, can be approximated by  $\Delta\Omega_0 \approx \Delta/(2b_0)$ . In our simulations we used  $\Delta = 0.03$  which leads to a frequency mismatch of  $\Delta\Omega_0 \approx 1.7\%$ .

Figure 6(a) plots the relative frequency difference  $\Delta\Omega(\varepsilon)$  for the two patch UPCA system (solid line). As  $\varepsilon$  increases, the frequency difference between the two patches reduces sharply and reaches zero at the critical coupling  $\varepsilon_c = 0.016$ . At this point one to one frequency locking is achieved and the two systems are phase synchronized.

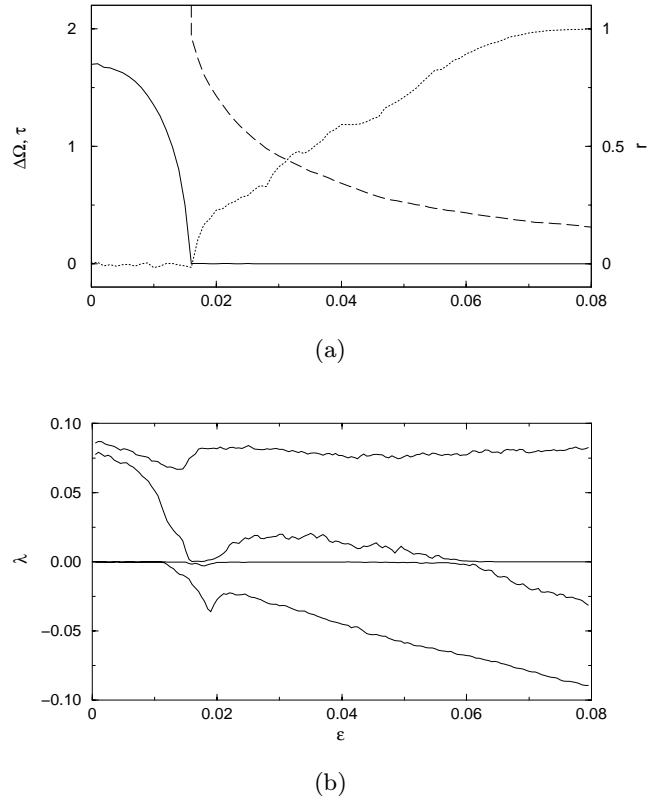


Fig. 6. Transition to phase synchronization for two coupled nonidentical foodweb systems ( $b_1 = 0.875$ ,  $b_2 = 0.845$ ), as a function of the coupling  $\varepsilon$ . (a) Relative frequency difference,  $\Delta\Omega$ , (solid line); phase lag,  $\tau$ , (rel. time units) (dashed line); correlation,  $r$ , between peak predator abundances (dotted line); calculated after initial transients removed. (b) The four largest Lyapunov exponents of the coupled two-patch system as a function of coupling  $\varepsilon$ .

The scaling of  $\Delta\Omega$  is very well approximated by the beat frequency of two diffusively coupled periodic oscillators

$$\Delta\Omega(\varepsilon) = \begin{cases} \Delta\Omega_0 \sqrt{1 - \varepsilon^2/\varepsilon_c^2}, & \varepsilon \leq \varepsilon_c \\ 0, & \varepsilon > \varepsilon_c \end{cases} \quad (11)$$

It is impossible from an examination of  $\Delta\Omega$  alone to discern at which point in the frequency locked regime full synchronization is achieved (i.e. where the amplitudes of the two systems are identical or highly correlated). For this reason the correlation  $r$  between the two predator time series  $w$  (i.e. the discretized maxima  $A_n$ ) is also plotted as a function of migration  $\varepsilon$  (dotted line). The figure shows that for migration larger than  $\varepsilon \gtrsim \varepsilon_f = 0.07$ , the patches are fully synchronized in phase and amplitude for both  $r = 1$  and  $\Delta\Omega = 0$ . Note that for intermediate coupling levels ( $\varepsilon_c < \varepsilon < \varepsilon_f$ ) there is a distinct regime of phase synchronization where  $\Delta\Omega = 0$ , but the

amplitudes of the two time-series are only weakly correlated.

In Fig. 6(a), we also plot the time lag (dashed line) between the two synchronized patches as a function of migration  $\varepsilon$ . The time lag appears with the creation of phase synchronization and tends to decrease with  $\varepsilon$  as full synchronization is approached. The region of full correlation between peak amplitudes ( $r = 1$ ) which are separated by time lags has been termed lag synchronization [Rosenblum *et al.*, 1997].

The Lyapunov spectra gives further insight into the synchronization transitions of chaotic systems [Rosenblum *et al.*, 1996, 1997]. Recall that since the uncoupled foodweb model is a three-dimensional dissipative chaotic system, it must have one positive, one negative, and one zero Lyapunov exponent (LE). In Fig. 6(b) we have plotted the four largest Lyapunov exponents for two coupled foodweb models [i.e. Eqs. (10)] as a function of the coupling strength  $\varepsilon$ . For this range in coupling, the foodwebs remain chaotic and the largest LE is always positive while the LE associated with the phase coordinate is zero. For weak coupling ( $\varepsilon < 0.011$ ), the two foodweb models are unsynchronized and there are two positive, two negative and two zero LE's. As the coupling is increased phase synchronization sets in at  $\varepsilon = \varepsilon_c$  and one zero LE becomes negative corresponding to a stable relationship between the phases of the two foodwebs. As coupling is increased even further, there is a transition to "full synchronization" which is characterized by a zero crossing of one of the positive exponents at  $\varepsilon = 0.062$ . The remaining single positive LE ensures that the amplitude dynamics are chaotic. The two negative LE's, on the other hand, indicate that now there is "full synchronization" in both phase and amplitude; the dynamics of the two oscillators have become almost, if not identical, to one another. The large dips in the LE spectra [Fig. 6(b)] at the transition to phase synchronization are due to the creation of periodic windows [Rosenblum *et al.*, 1996].

We also examined the more complicated phase synchronization of coupled "funnel" oscillators [Osipov *et al.*, 1997]. Recall that the small and large loops of the funnel attractor [Fig. 2(b)] may be associated with their own characteristic period lengths [Fig. 4(d)]. The smaller loops (which do not occur in the phase coherent attractor) are induced whenever the peak value of  $w$  increases above a certain threshold level  $A_{th} = 2.1$  for the parame-

terization of Fig. 4(d). These above threshold peaks have the potential to interfere with the synchronization as shown in Fig. 7(a), where the time-series of two nonidentical systems (funnel regime) are plotted for a relatively large coupling ( $\varepsilon = 0.75$ ). Here we use values of  $b_0 = 0.935$  and  $\Delta = 0.03$  so that the funnel oscillators are far away from any periodic windows. As long as both systems have comparable periods the two systems remain synchronized. But occasionally, the amplitude in one oscillator exceeds the threshold level  $A_{th}$ , while the amplitude of the other oscillator is subthreshold [indicated by the arrow in Fig. 7(a)]. This leads to a large difference of the period length and instantaneous frequency of the two systems in the following cycle; a situation which drives the two systems out of synchronization. After a short transient of some cycles, in which the two systems are clearly not locked, synchronization is returned once again. This short desynchronization event leads to a phase-slip of  $2\pi$  between the phases. Hence the two coupled "funnel" oscillators may be phase synchronized for extended periods of time, but these bouts of synchronization are repeatedly interrupted by short segments of desynchronization.

As in the phase coherent regime, we again plot the Lyapunov spectra of the two coupled funnel systems as a function of the coupling [Fig. 7(b)]. Since the LE are independent of a particular choice of phase variable, this method should provide an appropriate measure to characterize the synchronization even in the less phase coherent funnel regime. Figure 7(b) shows that the Lyapunov spectra change with the coupling parameter exactly as is typical for the transition to phase synchronization [compare with Fig. 6(b)] [Rosenblum *et al.*, 1996]. Thus, in analogy to the phase coherent regime, one might expect that the zero crossings of the LE's indicate the onset of phase synchronization ( $\varepsilon = 0.035$ ) and full synchronization ( $\varepsilon = 0.115$ ).

However this proves not to be the case. For coupling of strength  $\varepsilon = 0.075$ , for example, the Lyapunov spectra might predict perfect phase synchronization. But, the corresponding time-series generated with  $\varepsilon = 0.075$  [Fig. 7(a)], clearly reveals the existence of segments with desynchronization events where phase synchronization breaks down. Thus the method of calculating Lyapunov spectra is not able to resolve the frequent desynchronization events that occur in the funnel regime, and so it can be a problematic guide for detecting phase synchronization. The problem stems from the

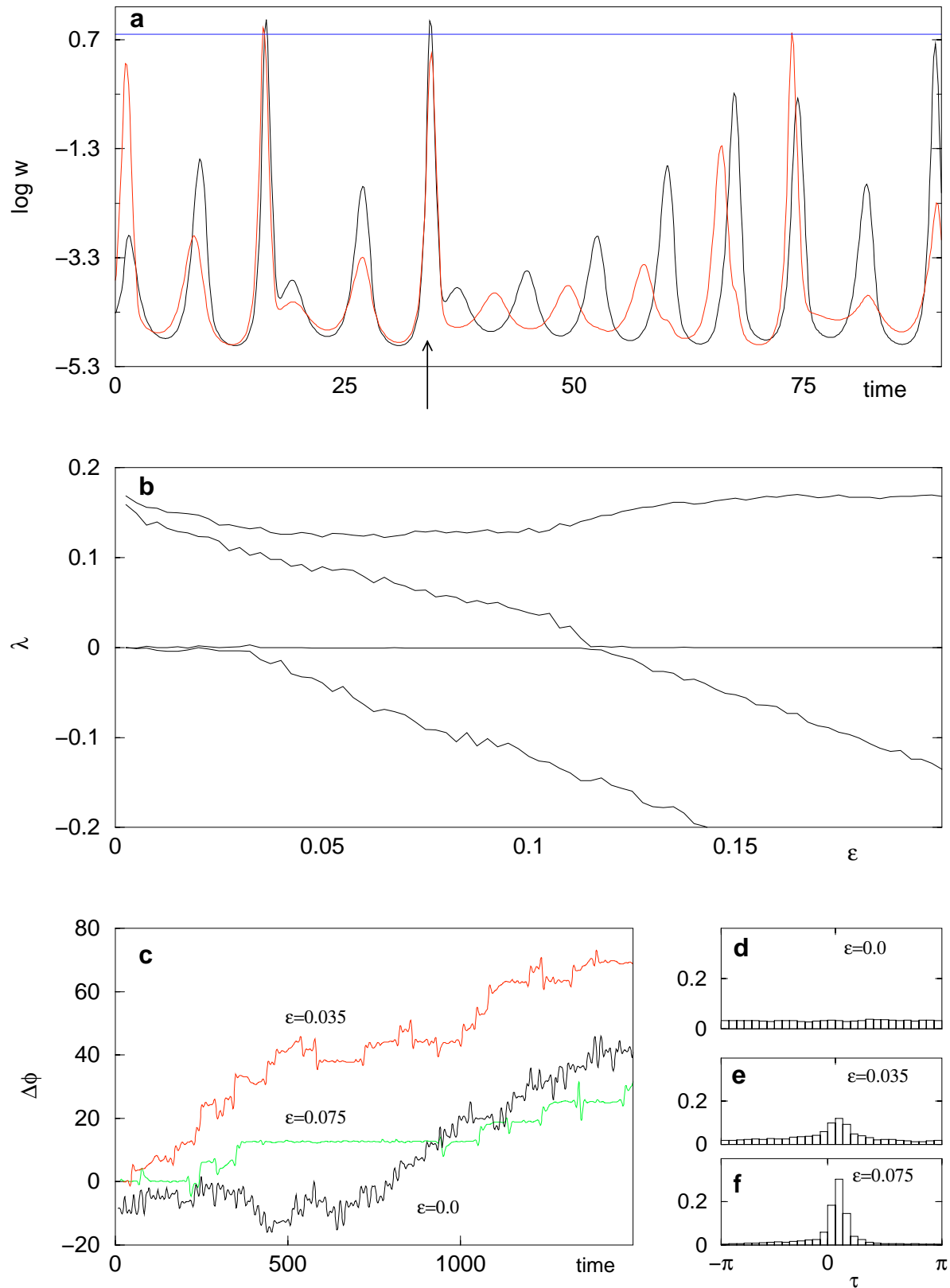


Fig. 7. Synchronization of two coupled nonidentical foodweb systems (10) in the “funnel” regime, ( $c = 12.3$ ,  $b_1 = 0.95$ ,  $b_2 = 0.92$ ) as a function of coupling  $\epsilon$ . (a) Time-series of top predators,  $w_i$  (black and red). Whenever one population exceeds the threshold level  $A_{th} = 2.1$  (horizontal line), a desynchronization event occurs; (b) four largest Lyapunov exponents; (c) phase difference,  $\Delta\phi$  for the coupling  $\epsilon = 0$  (black),  $\epsilon = 0.035$  (red) and  $\epsilon = 0.075$  (green). Distribution of relative phase difference  $\tau = \Delta\phi \bmod 2\pi$  for (d)  $\epsilon = 0$ , (e)  $\epsilon = 0.035$  and (f)  $\epsilon = 0.075$ .

method of calculating Lyapunov exponents which averages over synchronized and unsynchronized trajectories.

We also plot the growth in the instantaneous phase difference  $\Delta\phi$  (Eq. 5) of the funnel oscillator, for different couplings [Fig. 7(c)]. In the uncoupled case ( $\varepsilon = 0$ ), the phase difference performs a random walk-like motion. For small levels of coupling (e.g.  $\varepsilon = 0.035$ ), regimes of phase-locking are initiated and the phase difference shows plateaus which are interrupted by phase slips. Stratanovich [1963] developed a method to investigate phase-locking in stochastic systems from the statistical distribution of the relative phase differences  $\tau = \Delta\phi \bmod 2\pi$ . Stratonovitch [1963] observed that synchronization appears as a peak in the distribution of the phase lags  $\tau$ . The same method is appropriate for studying the synchronization of the coupled funnel oscillators which appear to phase synchronize intermittently. For the case of no coupling ( $\varepsilon = 0$ ) and thus in the absence of synchronization, the lags  $\tau$  are uniformly distributed [Fig. 7(d)]. For the higher coupling ( $\varepsilon = 0.035$ ) a peak is seen in the distribution of  $\tau$  [Fig. 7(e)]. For even stronger coupling ( $\varepsilon = 0.075$ ) the amplitudes become highly correlated, and the chance that the amplitude of only one of the systems increases above the threshold is very small. As a result the phase slips become more and more rare [Fig. 7(f)]. A deeper understanding of this “imperfect” phase synchronization can be obtained by an analysis of the unstable periodic orbits [Zaks *et al.*, 1999].

## 5. Influence of Noise

The deterministic foodweb model Eq. (1) should be viewed as a mean field approximation of averaged variables in a stochastic and homogenous mixing population. But even though the equations are designed to simulate the stochastic scenario, the mean field approximation can break down when population levels reach low values. In these circumstances, it is useful to insert additive demographic noise to those variables which reach critically low levels (see [May, 1974]). The equations with this demographic stochasticity read as follows:

$$\begin{aligned} \dot{u} &= a(u - u^*) - \alpha_1 f_1(u, v) + \eta_1 \\ \dot{v} &= -b(v - v^*) + \alpha_1 f_1(u, v) - \alpha_2 f_2(v, w) + \eta_2 \\ \dot{w} &= -c(w - w^*) + \alpha_2 f_2(v, w) + \eta_3. \end{aligned} \quad (12)$$

Additive noise  $\eta_i$  is applied simultaneously to all variables. Here  $\eta$  is taken from a normal distribution with  $\langle \eta_i \rangle = 0$  and  $\langle \eta_i(t_1)\eta_i(t_2) \rangle = D^2\delta \times (t_2 - t_1)$ , but in order to obtain strictly positive population numbers, the noise is restricted, so that at any time  $\eta_3(t) + w(t) \geq 0$ . The stochastic equations are numerically solved using an Euler scheme with a step size of  $dt = 0.001$ .

We have observed a number of noise-induced phenomena that arise in Eqs. (12). Of particular interest is the manner in which demographic noise induces UPCA-like oscillations for parameter regimes that would otherwise be periodic, thus significantly broadening the range in parameter space for which there is UPCA. To demonstrate this, the model was parameterized to give limit cycle behavior in the absence of noise by reducing  $b$  from  $b = 1$  (UPCA chaos) to  $b = 0.2$  [limit cycle, see bifurcation diagram Fig. 3(a)].

Initially the equations were integrated without demographic noise and, as Fig. 8(a) displays, the predator population ( $w$ ) oscillates periodically. At  $t = 50$ , however, demographic noise with strength  $D = 0.04$  was switched on, causing the appearance of strong chaotic fluctuations in the amplitudes. The noise-induced oscillations are phase coherent and have characteristics associated with UPCA. Similar noise induced UPCA has been previously observed with the introduction of environmental (multiplicative) noise [Blasius *et al.*, 1999].

We investigated the noise dependence of the UPCA-like oscillations by plotting the variance,  $\sigma$ , of the maxima of  $w$  and the diffusion constant,  $D_\phi$ , as a function of noise-strength  $D$ . Figure 8(b) shows that the UPCA dynamics is induced smoothly without any threshold effect (soft induction) [Deissler & Farmer, 1992]. The noise-induced variance in the peak amplitudes saturates at noise levels of about  $D = 0.04$ . In Fig. 5(b) the phase diffusion of the noise forced model is compared with strictly deterministic systems. The phase coherency induced by a noise level of  $D = 0.04$  corresponds roughly to the phase coherency found in the “funnel” regime. Hence one should expect to find similar transitions to synchronization for these two different types of systems.

The effects of noise on synchronization of two coupled UPCA models are explored by monitoring the growth in phase difference between two coupled foodweb models (Fig. 9). The noise level  $D$  was set at 10% of the population mean, which in the case of the predator population  $w$  corresponds to

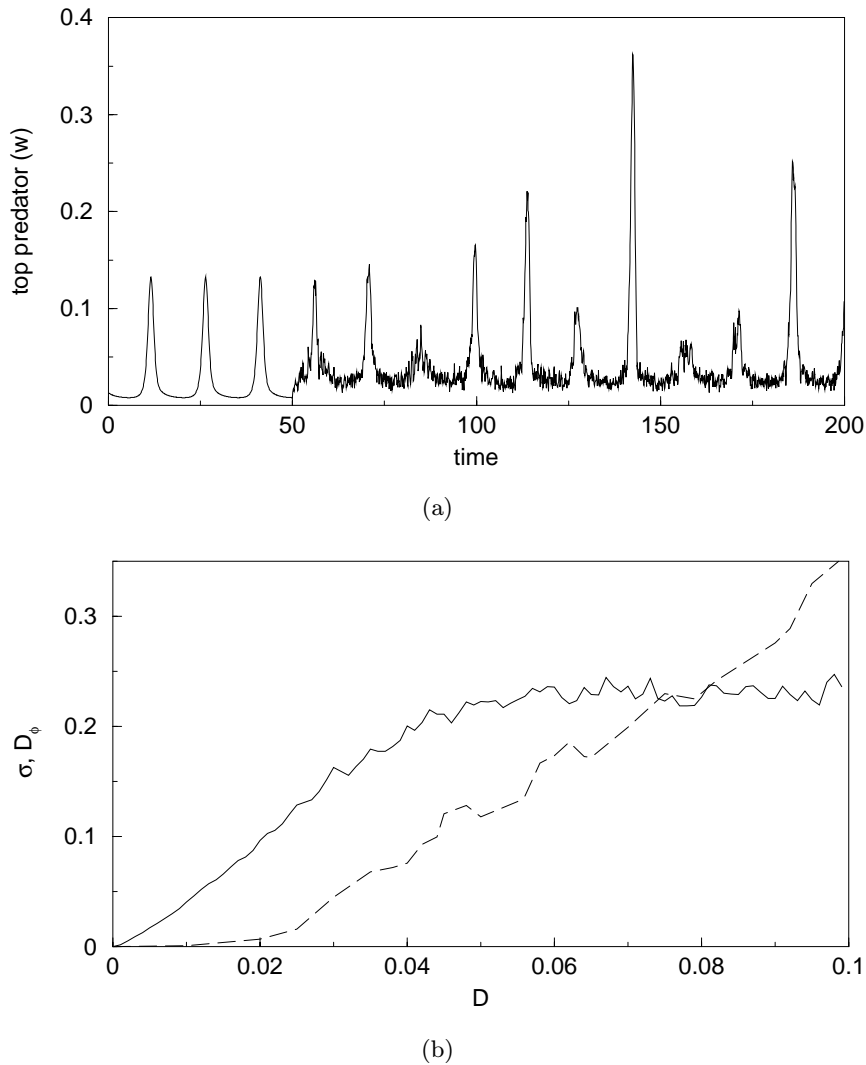


Fig. 8. Noise-induced UPCA in the foodweb model (1). The system is parameterized on the limit cycle regime with  $b = 0.2$ . (a) At  $t = 50$  additive noise is introduced with strength  $D = 0.04$  and UPCA oscillations result. (b) Standard deviation of peak amplitudes,  $\sigma$ , and phase diffusion,  $D_\phi$ , Eq. (9) as a function of noise strength  $D$ .

$D = 0.08$ . This has been done for the couplings of  $\varepsilon = 0$ ,  $\varepsilon = 0.05$  and  $\varepsilon = 0.1$  as well as for the reference case of an uncoupled ( $\varepsilon = 0$ ) system without noise which gives an almost linear phase growth in phase difference. One clearly observes that without coupling, the noise forced trajectory follows a random walk about the linear growth associated with the zero noise reference. For higher coupling phase locking is initiated and the phase growth tends to be stationary but is erratically interrupted by phase slips where the phase jumps up or down by  $2\pi$ . One sees from Fig. 9(a) that the higher the coupling, the smaller is the rate of occurrence of phase slips.

It is possible to check the influence of noise forcing on the phase synchronization from an examination of the statistical distribution of the

relative phase lag  $\tau$  between the closely (but not perfectly) locked populations [Tass *et al.*, 1998] (as in Sec. 4 for the funnel attractor). Recall that for a purely deterministic synchronized system the populations cycle are separated by a stable phase lag  $\tau_0$ . In the absence of synchronization the distribution of the phase lag  $\tau$  between two noise forced patch populations is that of a uniform random variable [Fig. 9(b),  $\varepsilon = 0.0$ ]. In contrast, phase synchronization is characterized by a distribution that is peaked at the phase lag  $\tau = \tau_0$  and  $\tau$  has the tendency to remain close to the “preferred” mean value  $\tau_0$  [Fig. 9(c),  $\varepsilon = 0.05$ ]. With higher coupling [Fig. 9(d),  $\varepsilon = 0.1$ ] the peak in the frequency histogram becomes even sharper. The statistical approach for detecting phase synchronization is

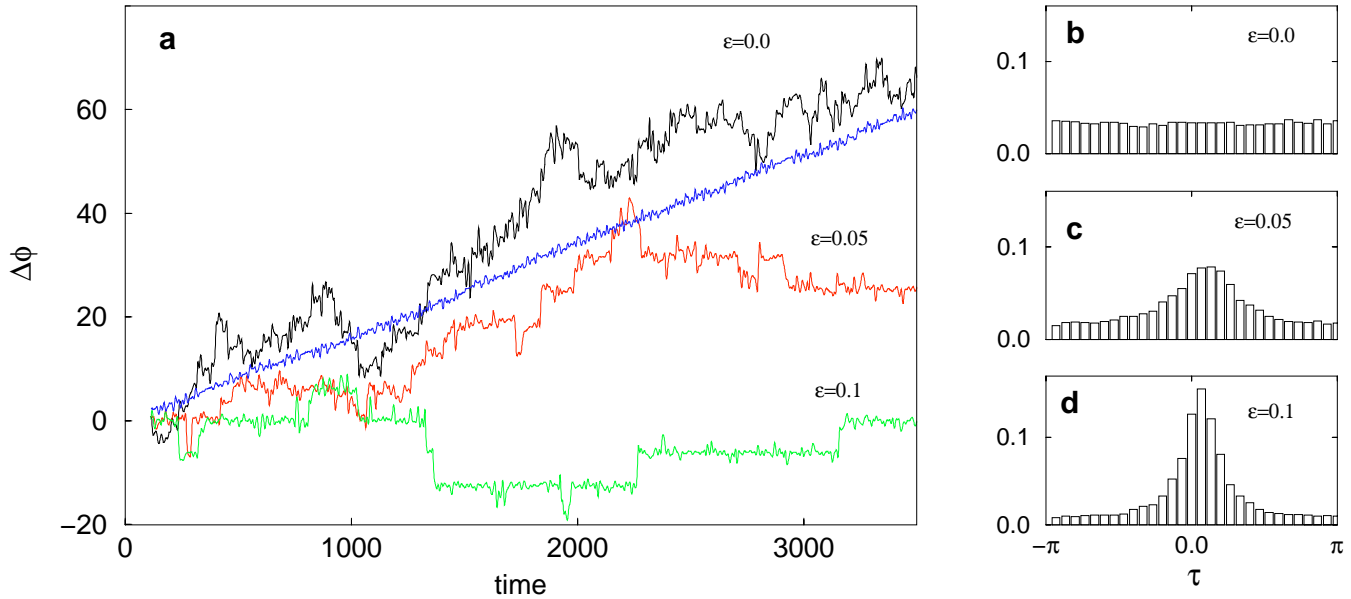


Fig. 9. (a) Growth of phase difference  $\Delta\phi$  of two coupled noise forced foodweb models in the phase coherent chaotic regime for ( $b_1 = 0.875$ ,  $b_2 = 0.845$ ). Additive demographic noise with standard deviation set at 10% of population mean. “Blue reference line” represents linear phase growth  $\Delta\phi$  for uncoupled purely deterministic foodweb models. Phase growth with demographic noise forcing: (i)  $\varepsilon = 0$  (black line) — random walk that hovers about “blue reference line”; (ii)  $\varepsilon = 0.05$  (red line) — the noise introduces phase slips which erratically increase  $\Delta\phi$ ; (iii)  $\varepsilon = 0.1$  (green line) — the increased coupling suppresses phase growth despite the additive noise. (b)–(d) A statistical description of synchronization is provided by the distribution of relative phase lags  $\tau$ .

thus successful for both noise forced phase coherent systems as well as weakly coherent systems such as the “funnel” attractor (as shown in Sec. 4).

## 6. Phase Synchronization in Spatially Extended Systems

We now study the synchronization of an ensemble of nonidentical foodweb systems which are coupled by diffusive migration. Here we are motivated by the unusual spatiotemporal synchronization observed in the Canadian hare–lynx cycle. Figure 10(a) shows the remarkably synchronized cycles of the lynx fur records in six geographically distinct regions in Canada. This is but a glimpse of a much larger picture in which hare and lynx populations across Canada synchronize in phase to a collective cycle that manifests over millions of square kilometers. Similar spatially synchronized fluctuations have been observed for many other ecological populations [Keith 1963; Korpimaki & Krebs, 1996; Ranta *et al.*, 1997].

To examine spatial synchronization, we constructed a lattice of  $N \times N$  patches, each patch consisting of the previously described three-trophic (vegetation–herbivore–predator) population model.

The model foodwebs were nonidentical, having random natural frequencies that act as spatial inhomogeneity over the lattice. In order to achieve this, the consumer growth rates  $b_i$  were taken from a uniform distribution within 10% (solid line Fig. 11) or 5% (dashed line Fig. 11) from the mean  $\langle b_i \rangle = 1$ . Each patch was connected to its eight nearest neighbors to take into account local migration  $\varepsilon$ . We performed a series of lattice simulations with free and periodic boundary conditions, and for lattices with  $N = 20, 50, 100$  and 200, and with coupling to four or eight nearest neighbors. All our main results were found to be robust to these changes in model configuration.

In Fig. 11 we examine synchronization of the  $20 \times 20$  lattice as a function of migration  $\varepsilon$ , similar to Fig. 6(a) for the two patch system. Now  $\Delta\Omega$  measures the standard deviation of the frequencies  $\Omega_i$  of all 400 patches as a percentage of the mean frequency. With no migration between patches ( $\varepsilon = 0$ ), the populations display independent chaotic oscillations, and frequencies vary with standard deviation  $\Delta\Omega = 0.28\%$ . However, with increasing coupling  $\Delta\Omega$  drops sharply. Finally, at  $\varepsilon_c = 0.025$  (solid line), the frequency difference,  $\Delta\Omega$ , between all patches reaches zero. At this small

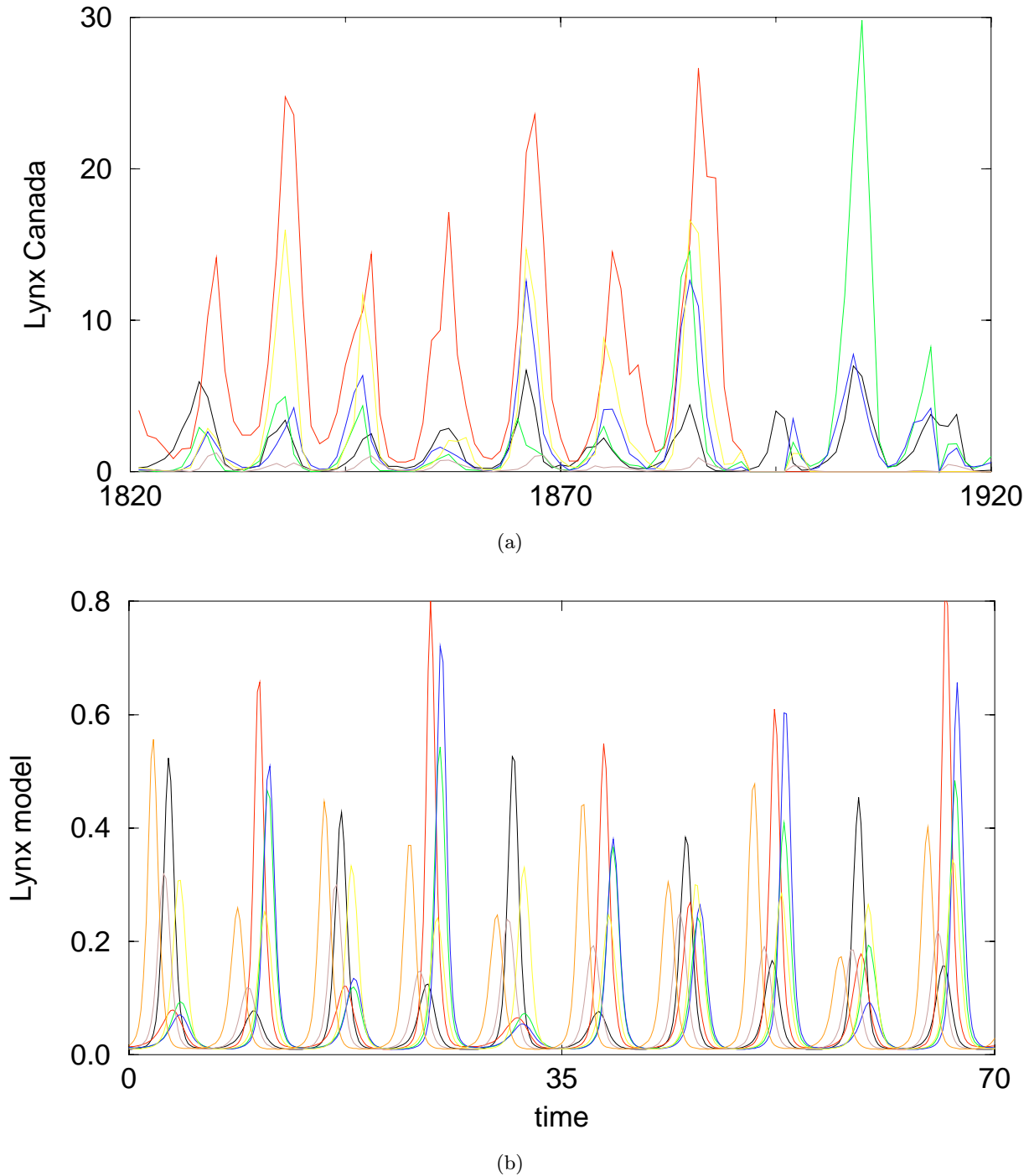


Fig. 10. (a) Time-series of Canadian lynx in six different regions in Canada after [Elton & Nicholson, 1942]. (b) Time-series of predator  $w$  in a  $20 \times 20$  lattice with next neighbor coupling ( $\varepsilon = 0.035$ ) and periodic boundary conditions. Time-series for seven patches spaced along the lattice diagonal.

level of migration, the whole lattice becomes globally phase synchronized to a common frequency. If the coupling is weak enough, the “peak amplitudes” of patch populations remain weakly correlated [see Fig. 10(b)].

It is this regime of strong phase-locking, but weakly correlated amplitudes, which resembles natural systems. In Fig. 10 we compare our lattice simulations with the synchronized oscillations in Canadian lynx. Similar to the real data,



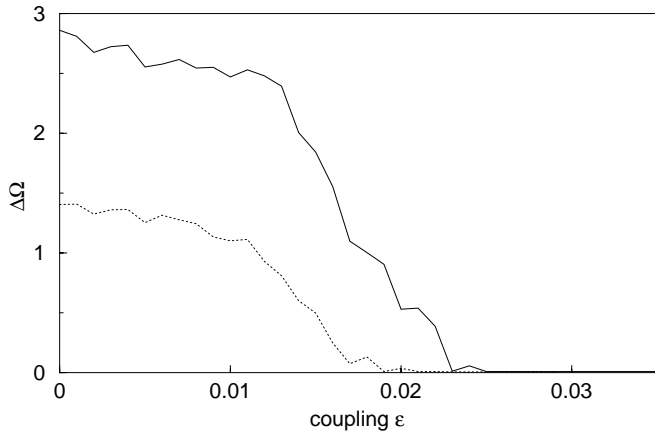


Fig. 11. Frequency difference from the mean in a  $20 \times 20$  lattice of foodweb models as a function of the coupling  $\varepsilon$ . Here  $\Delta\Omega$  measures the standard deviation of frequencies  $\Omega_i$  for all 400 patches as a percent of the mean frequency. The consumer growth rates  $b_i$  of the foodwebs were uniformly distributed in the interval  $[0.9, 1.1]$  (solid line) and  $[0.95, 1.05]$  (dotted line).

despite the strong phase-locking, the amplitudes of patch populations remained only weakly correlated ( $r < 0.2$ ).

Note that for spatially extended systems full synchronization leads only to trivial spatial patterns, since phase and amplitude dynamics are then identical across the entire lattice. In the region of phase synchronization, however, synchronized patch populations are typically separated by a phase lag  $\tau_i$  [as seen in Fig. 6(a)]. When viewed over the whole lattice the time lags can show a characteristic “U” shape. In Fig. 12 we plot the convergence to the U-shape steady state as expressed through the time delay  $\tau_i$  between patches along the diagonal of the  $20 \times 20$  patch lattice system. Even though phase synchronization is almost immediate, relaxation to the U-state can take some 100 full cycles ( $t \approx 700$ ) to achieve.

The distribution of the phase lags gives rise to complex spatiotemporal patterns. Most remarkably, we find a coherent regular traveling wave structure where population abundances remain chaotic, but unusual circular waves form and spread in time across the spatial landscape (Fig. 13). The wave pattern repeats in an endless cycle, with patches having chaotic amplitudes,

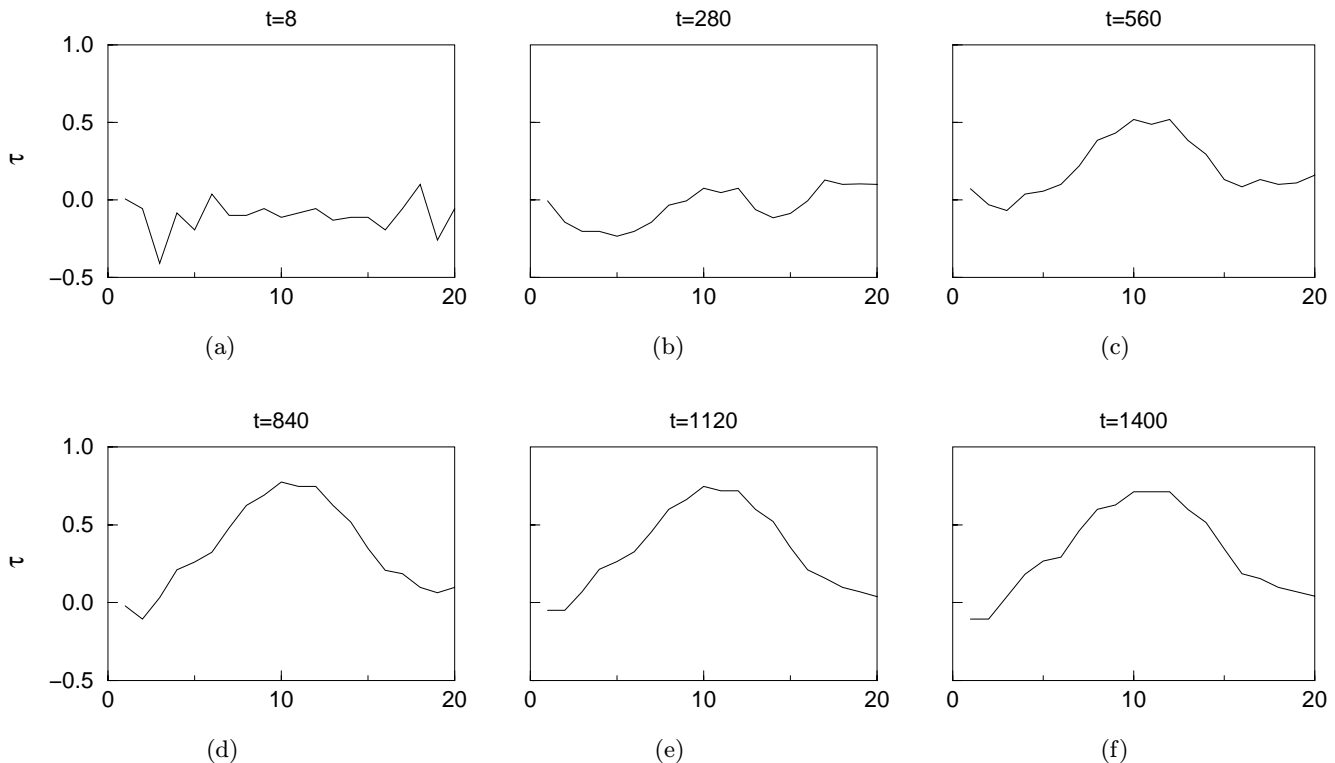


Fig. 12. Convergence to the U-shape steady state as expressed through the phase lag  $\tau$  between patches in the  $20 \times 20$  lattice parameterized as in Fig. 10. Each successive figure (a) to (f) is a snap-shot of the lattice phase relationship after running the model for 40 population cycles. Horizontal axis represents patch 1–20 along the lattice diagonal. Vertical axis  $\tau$  represents the fixed phase lag (with respect to the central patch) determined after the lattice has reached global phase synchronization. Note that the phase lag is plotted in units of  $2\pi$  (i.e.  $\tau = 1$  corresponds to a lag of  $2\pi$ ).

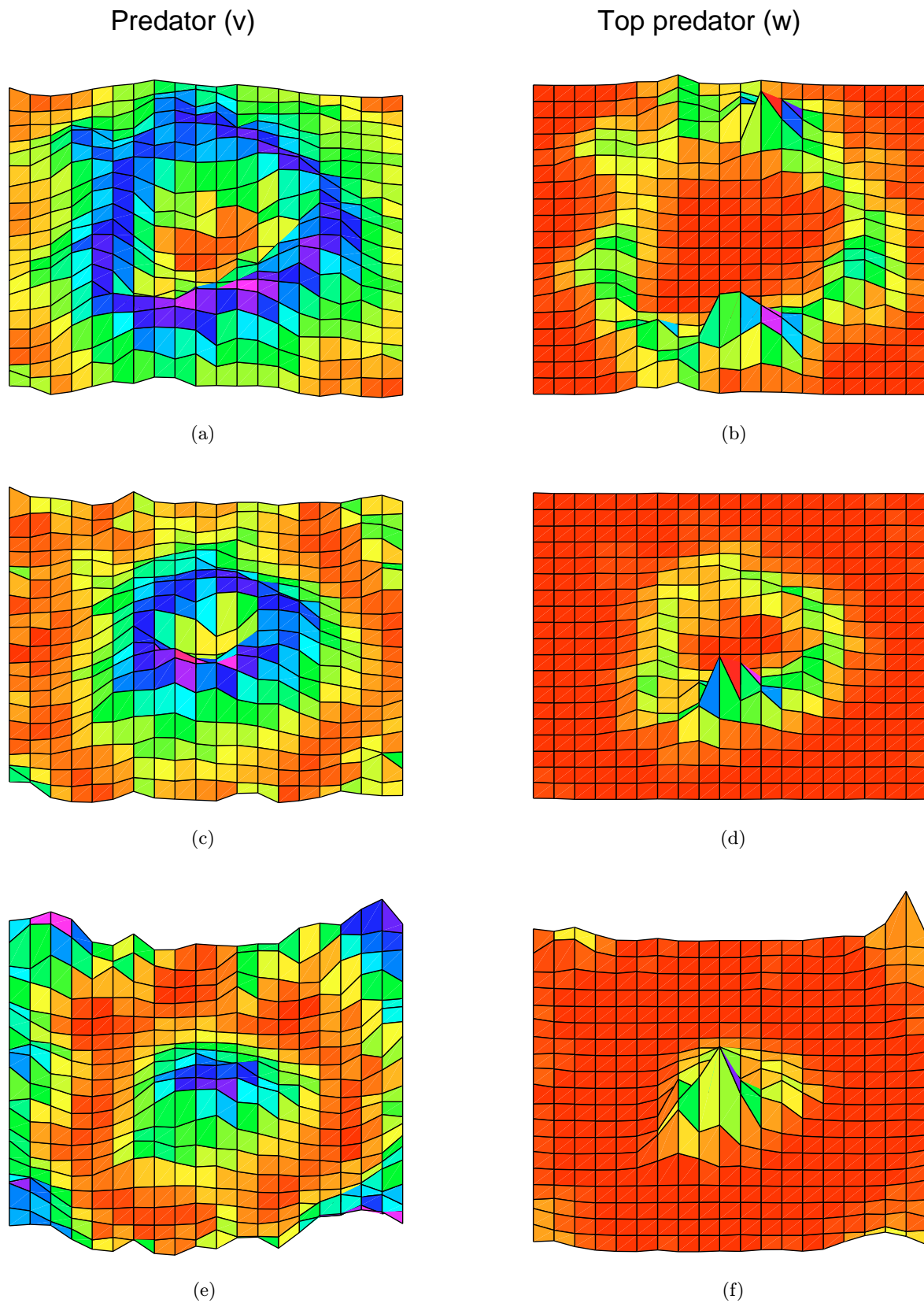


Fig. 13. Evolution of a chaotic ring wave. Snapshots of predators  $v_i$  (left column) and top predators  $w_i$  (right column) in a  $20 \times 20$  lattice [see Fig. 10(b) legend] for three consecutive time steps. Abundance levels are color coded.

making each cycle different from the next. In Fig. 13 we compare typical waves which arise in the smooth varying  $v$ -variable (left column) with the more spiky  $w$ -variable (right column). One sees that the sharp spike train of  $w$  in time translates as a sharp structure in the spatial domain. In our numerical investigations, we found the chaotic ring waves only in the regime of global phase synchronization with weakly correlated patch amplitudes. Recent ecological field studies have reported similar traveling wave structures with spatially distributed U-shaped phase lags [Ranta & Kaitala, 1997].

## 7. Discussion

We have presented a simple biologically realistic foodweb model that exhibits UPCA dynamics similar to that found in the chaotic Rössler system. The regular frequency of the population oscillations combined with the chaotic amplitudes of each cycle are properties that should be relevant for describing many ecological and biological scenarios. Similar UPCA-like oscillations are also induced by external noise for parameter regimes that would otherwise be periodic, thus significantly broadening the biologically relevant range in parameter space. Furthermore, the minimal structure of the model suggests that there exists a larger class of related systems which can qualitatively reproduce similar chaotic UPCA dynamics.

It was possible to capture the complex dynamics of the continuous time UPCA models with only two simple discrete maps; the first  $F$ , describing the amplitude dynamics, and a second,  $G$ , which describes the phase evolution through its dependence on amplitude. The map  $G$  allows classification of different types of UPCA (e.g. phase coherent versus “funnel”). In addition, given the two maps it is possible to directly calculate many interesting quantities without having to numerically integrate the foodweb model directly. Our future goal is to explore whether the synchronization properties of the continuous time model can be understood from the discrete maps alone. If so, the synchronization of different types of systems (e.g. phase coherent systems, two frequency systems . . .) may be derived from the maps without having to deal with the continuous time equations.

We have attempted to investigate the spatio-temporal dynamics of synchronization in higher dimensional lattices of nonidentical chaotic systems — an area that to date is almost completely unex-

plored. It was found that phase synchronization in two-dimensional lattices of coupled foodweb oscillators manifests spatially as regular circular traveling waves in which oscillator amplitudes are chaotic and poorly correlated. Similar chaotic waves have also been noted in one-dimensional circular lattices [Blasius *et al.*, unpublished], for different parameterizations of the foodweb model (e.g. for Lotka–Volterra or Holling type II interaction), and also in coupled Rössler systems. Thus the phenomenon is robust and one could expect that it emerges in a generic way. The chaotic traveling waves do not appear to have been noted in the literature previously. We now believe that the conditions in which they arise depend crucially on the spatial frequency “inhomogeneity,” as will shortly be reported [Blasius *et al.*, unpublished]. The chaotic waves pose many other questions. Are there regimes in which different wave forms arise such as spiral or planar waves? Can one characterize the waves in terms of wavelength, velocity, dispersion relations, wave front width etc., and study their dependence on initial and boundary conditions? Then there are ecological concepts that may be addressed. For example, we are led to believe that these wave structures, and more generally spatial phase synchronization, plays an important role in preventing species extinctions. Yet conventional wisdom dictates that the synchronization of populations leads to an increase of extinction risk. These and many other exciting themes are waiting further exploration with the chaotic foodweb model described here.

## Acknowledgments

We thank Jürgen Kurths for his strong encouragement, and Amit Huppert for many helpful discussions. B. Blasius was supported by a Minerva Fellowship. We are grateful for support from the Adams Super Center for Brain Studies at Tel Aviv University and an internal Tel Aviv University grant.

## References

- Blasius, B., Huppert, A. & Stone, L. [1999] “Complex dynamics and phase synchronization in spatially extended ecological systems,” *Nature* **399**, 354–359.
- Blasius, B. & Stone, L. [1999] “Chaotic waves and phase synchronization in spatially extended ecological systems,” in *Stochaos: Stochastic and Chaotic Dynamics in the Lakes*, eds. Broomhead, D. S., Luchinskaya,

- E. A., McClintock, P. V. E. & Mullin, T. (American Institute of Physics, Woodbury, NY), **502**, pp. 221–225.
- Blasius, B. & Stone, L. [2000] “Nonlinearity and the Moran effect,” *Nature* **406**, 846–847.
- Deissler, R. J. & Farmer, J. D. [1992] “Deterministic noise amplifiers,” *Physica* **D55**, 155–165.
- Elton, C. & Nicholson, M. [1942] “The ten-year cycle in numbers of the lynx in Canada,” *J. Anim. Ecol.* **11**, 215–244.
- Farmer, J. D., Crutchfield, J., Froeling, H., Packard, N. & Shaw, R. [1980] “Power spectra and mixing properties of strange attractors,” *Ann. NY Acad. Sci.* **357**, 453–472.
- Farmer, J. D. [1981] “Spectral broadening of period-doubling bifurcation sequences,” *Phys. Rev. Lett.* **47**, 179–182.
- Fujisaka, H. & Yamada, T. [1983] “Stability theory of synchronized motion in coupled-oscillator systems,” *Progr. Th. Phys.* **69**, p. 32.
- Gabor, D. [1946] “Theory of communication,” *J. IEEE London* **93**, 429–457.
- Hastings, A. & Powell, T. [1991] “Chaos in a three-species food chain,” *Ecology* **72**, 896–903.
- Huygens, C. H. [1673] *Horologium Oscilatorium* (Parisii, France).
- Keith, L. B. [1963] *Wildlife’s Ten Year Cycle* (University of Wisconsin Press, Madison).
- Korpimäki, E. & Krebs, C. J. [1996] “Predation and population cycles of small mammals. A reassessment of the predation hypothesis,” *BioScience* **46**, 754–764.
- Levin, S. A., Grenfell, B., Hastings, A. & Perelson, A. S. [1997] *Science* **275**, 334–343.
- May, R. [1974] *Stability and Complexity in Model Ecosystems* (Princeton University Press, Princeton, NJ).
- Parlitz, U., Junge, L., Lauterborn, W. & Kocarev, L. [1996] “Experimental observation of phase synchronization,” *Phys. Rev.* **E54**, 2115–2118.
- Pecora, L. M. & Carroll, T. L. [1990] “Synchronization in chaotic systems,” *Phys. Rev. Lett.* **64**, p. 821.
- Pikovsky, A. S. [1984] “On the interaction of strange attractors,” *Z. Physik* **B55**, 149–154.
- Pikovsky, A. S., Rosenblum, M. G., Osipov, G. V. & Kurths, J. [1997] “Phase synchronization of chaotic oscillators by external driving,” *Physica* **D104**, 219–238.
- Ranta, E. & Kaitala, V. [1997] “Traveling waves in vole population dynamics,” *Nature* **390**, p. 456.
- Ranta, E., Kaitala, V. & Lundberg P. [1997] “The spatial dimension in population fluctuations,” *Science* **278**, 1621–1623.
- Rössler, O. E. [1976] “An equation for continuous chaos,” *Phys. Lett.* **A57**, 397–398.
- Rosenblum, M. G., Pikovsky, A. S. & Kurths, J. [1996] “Phase synchronization of chaotic oscillators,” *Phys. Rev. Lett.* **76**, 1804–1807.
- Rosenblum, M. G., Pikovsky, A. & Kurths, J. [1997] “From phase to lag synchronization in coupled chaotic oscillators,” *Phys. Rev. Lett.* **78**, 4193–4196.
- Rosenblum, M. G. & Kurths, J. [1998] “Analyzing synchronization phenomena from bivariate data by means of the Hilbert transform,” in *Nonlinear Analysis of Physiological Data*, eds. Kantz, H., Kurths, J. & Mayer-Kress, G., Springer Series for Synergetics, pp. 91–99.
- Rulkov, N. F., Sushchik, M. M., Tsimring, L. S. & Abarbanel, H. D. I. [1995] “Generalized synchronization of chaos in directionally coupled chaotic systems,” *Phys. Rev.* **E51**, 980–994.
- Schäfer, C., Rosenblum, M. G., Kurths, J. & Abel, H.-H. [1998] “Heartbeat synchronized with ventilation,” *Nature* **392**, 239–240.
- Schaffer, W. M. [1984] “Stretching and folding in lynx fur returns: Evidence for a strange attractor in nature?” *Am. Nat.* **124**, 798–820.
- Stone, E. [1992] “Frequency entrainment of a phase coherent attractor” *Phys. Lett.* **A163**, 367–374.
- Stone, L. [1993] “Period-doubling reversals and chaos in simple ecological models,” *Nature* **365**, 617–620.
- Stratonovich, R. L. [1963] *Topics in the Theory of Random Noise* (Gordon and Breach, NY).
- Takens, F. [1981] “Detecting strange attractors in turbulence,” in *Dynamical Systems and Turbulence* eds. Rand, D. A. & Young, L.-S., Springer Lecture Notes in Mathematics, Warwick **898**, pp. 366–381.
- Tass, P., Rosenblum, M. G., Weule, J., Kurths, J., Pikovsky, A. S., Volkman, J., Schnitzler, A. & Freund, H.-J. [1998] “Detection of  $n:m$  phase locking from noisy data: Application to magnetoencephalography,” *Phys. Rev. Lett.* **81**, 3291–3294.
- Osipov, G. V., Pikovsky, A. S., Rosenblum, M. G. & Kurths, J. [1997] “Phase synchronization effects in a lattice of nonidentical Rössler oscillators,” *Phys. Rev.* **E55**, 2353–2361.
- Yalcinkaya, T. & Lai, Y.-C. [1997] “Phase synchronization of chaos,” *Phys. Rev. Lett.* **79**, 3885–3888.
- Zaks, M. A., Park, E.-H., Rosenblum, M. G. & Kurths, J. [1999] “Alternating locking ratios in imperfect phase synchronization,” *Phys. Rev. Lett.* **82**, 4228–4231.